ACS OMEGA

Open Access

http://pubs.acs.org/journal/acsodf

Article

Phage Display Screening of Anchor Peptides for Red Blood Cell-Derived Extracellular Vesicles

Limei Xu, Xiao Xu, Jiang Xia, Huawei Zhang, Yujie Liang,* and Li Duan*

Cite This: *ACS Omega* 2024, 9, 6492−6504

Read Online

ACCESS | Metrics & More | Article Recommendations | Supporting Information

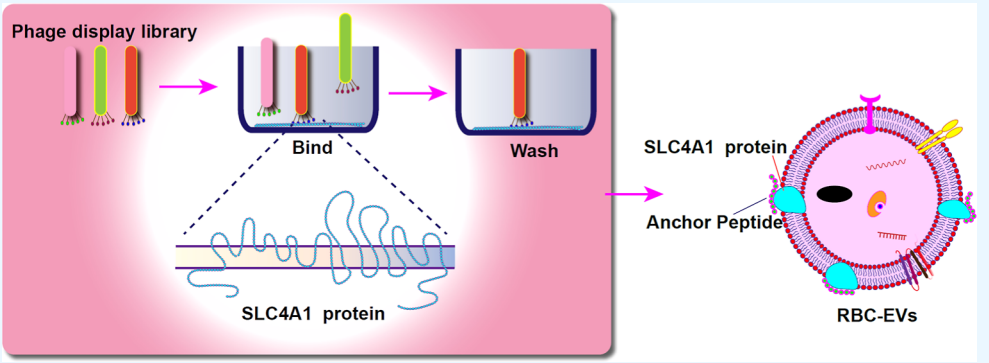

ABSTRACT: Extracellular vesicles (EVs) are increasingly used for disease diagnosis and treatment. Among them, red blood cell-derived EVs (RBC-EVs) have attracted great attention due to their abundant sources and low risks of gene transfer (RBC-EVs lack nuclear and mitochondrial DNA). Here, we first revealed the high expression level of membrane protein solute carrier family 4 member 1 (SLC4A1) in RBC-EVs through proteomic analysis. We then identified several binding peptides with high affinity for the SLC4A1 extracellular domain (SLC4A1-EC) from phage display library screening. A high affinity of SLC4A1-EC and the three peptides (XRB2, XRE4, and XRH7) were assessed in vitro using surface plasmon resonance analysis and SDS−polyacrylamide gel electrophoresis (SDS−PAGE). The binding sites of SLC4A1-EC and polypeptides were further predicted by LigPlot + analysis, and the results showed that these three polypeptides could bind to part of the hydrophobic residues of SLC4A1-EC. The binding efficiency of the anchor peptides to the RBC-EVs was further verified by flow cytometry and fluorescence imaging. In conclusion, we successfully screened three specific RBC-EV-targeting peptides which could potentially be utilized for isolating RBC-derived EVs from serum samples. More importantly, this peptide could be coupled with targeting peptides to modify RBC-EVs for drug delivery. Our work will provide a viable method for optimizing the function of RBC-EVs.

INTRODUCTION

Extracellular vesicles (EVs) are membranous vesicles released by cells into the extracellular space under physiological or pathological conditions, allowing cells to exchange proteins, lipids, and genetic materials.[1] Since EVs exhibit low levels of immunogenicity, good stability, and biocompatibility, EV or biomimetic exosome has shown broad application prospects in the field of drug delivery.[2−4] Studies have shown that drug delivery by pre-loading methods (e.g., manipulating the originating cell to overexpress therapeutic cargo) or post-loading methods (e.g., electroporation, incubation, and extrusion) into EVs has become a key cell-free therapeutic strategy for a range of diseases.[5,6]

Mesenchymal stem cells (MSCs) are multifunctional stem cells in multiple human tissues. MSC-derived EVs (MSC-EVs) not only have the same effects as MSCs but also have the advantages of low immunogenicity, good tolerance, and high repairability.[7,8] However, most methods for producing and purifying MSC-EVs lack standardization and quality control. In addition, most results are from in vitro or animal studies. The clinical safety of MSC-EVs needs further investigation.[9] In contrast, red blood cells (RBCs) are the most abundant cell type in the human body, and their safety has been proven in routine blood transfusions. More importantly, since mature RBCs lack nuclear and mitochondrial DNA, RBC-derived EVs (RBC-EVs) do not cause DNA contamination and lack transcription risks.[10] Previous studies on RBC-EVs have focused more on their function, and some studies have shown that RBC-EVs may be involved in the immune response to blood transfusion, but this may be related to the long-term

Received: August 31, 2023
Revised: December 26, 2023
Accepted: January 3, 2024
Published: January 31, 2024

storage of RBCs before blood transfusion. Currently, an increasing number of studies have focused on RBC-EVs as nanodrug delivery vehicles for drug delivery. One study showed that immRNA and 3p-125b-ASO delivered by RBC-EVs could trigger the RIG-I pathway and induce mouse and human breast cancer cell death. The therapeutic effect of this treatment method will be significantly improved if we can achieve targeted drug delivery to tumor cells.[11] Genetic engineering and chemical strategies have been extensively adopted to modify EVs with targeted ligands for delivering drugs to specific tissues or cells.[12−15] Since RBCs do not possess a nucleus, RBC-EVs can only be chemically modified by conjugating or lipid assembly of the targeted ligands.[16] The CP05 peptide, identified by phage display, enables the targeting and capture of exosomes from diverse origins by binding to CD63.[17] In our previous study, we employed CP05-coupled TRAP-binding peptide (TBP), a bifunctional peptide, TBP-CP05, which binds to CD63 on RBCEVs and receptors on osteoclasts, and used RBCEVs as a carrier to achieve the targeting of osteoclasts for the delivery of anti-miR-214 for the treatment of osteoporosis.[18] CD63 is a protein with four transmembrane domains enriched on the surface of exosomes and is regarded as an exosomal marker.[19] However, due to the heterogeneity of EVs, the expression level of CD63 in EVs from different sources is unstable, e.g., very low in EVs from human plasma.[20]

In this study, we tried to find a membrane protein with high specific expression on the surface of RBC-EVs, screened its specific binding peptide for the extracellular region of the membrane protein and predicted that the binding peptide could be applied to the targeted modification of RBC-EVs. We first compared the proteomics of human RBC-EVs and synovial fluid-derived MSC-EVs and found that the expression of CD63 in RBC-EVs was significantly lower than that in MSC-EVs. Nevertheless, the expression of solute carrier family 4 member 1 (SLC4A1) in the RBC-EVs increased significantly. SLC4A1 is a crucial transmembrane glycoprotein on the surface of the RBC membrane that is essential for maintaining the double-concave disk shape of RBCs.[21] To find RBC-EV-specific binding peptides, we panned the SLC4A1 extracellular domain (SLC4A1-EC) binding peptides by phage display technology. We then performed preliminary binding identification of the screened peptides to the SLC4A1 protein on EVs. Additionally, we predicted the binding sites of SLC4A1-EC and the screened peptides. The SLC4A1-specific binding peptides screened in this study will provide a potential tool to develop a RBC-EV-based drug-targeted delivery system.

MATERIALS AND METHODS

Preparation and Purification of EVs. Human peripheral blood and synovial fluid samples were approved by the ethics committee of Shenzhen Second People's Hospital (ethics number: 20220518003), and all the participants signed a written informed consent. Peripheral blood was collected from three healthy volunteers, and RBCs were separated by Ficoll−Paque PLUS (GE, USA). The RBCs were washed twice with PBS, and the residual leukocytes were filtered with a leukocyte filter (PALL, USA). The RBCs were finally resuspended in PBS and cultured overnight at 37 °C. The synovial fluid of three patients with osteoarthritis was collected. Our previous study found that MSCs derived from synovial fluid from patients with osteoarthritis had the typical immunophenotype and multidirectional differentiation potential of MSCs.[22] The MSCs were cultured according to the method in reference,[6] and P2−3 generation MSC culture medium was obtained. When the cells were collected, both RBCs and MSCs were in a viable state. The cells grew vigorously, the edges were clear, and the culture medium was clear and transparent. The collected human RBCs and MSC culture medium were centrifuged at 600g for 15 min, 2200g for 15 min, 3200g for 15 min, and 10000g for 30 min (rotor SW 32Ti, tube 38.6 mL, open, 4 °C) to remove cells and impurities. The supernatant was transferred to a fresh tube, filtered with a 0.22 μm filter, and then ultracentrifuged at 120,000 g for 70 min (rotor SW 32Ti, tube 38.6 mL, open, 4 °C) to collect the EV pellet which was then washed with PBS, resuspended in PBS, and placed in a −80 °C freezer for later use.

Characterization of EVs. EV size distribution was analyzed with a nanoparticle particle size analyzer (NS300, Malvern, England), NTA version (NTA 3.4—Sample Assistant Build 3.4.003-SA). Briefly, EVs were diluted with distilled water to 10^7−10^9/mL particles, and the detection threshold was adjusted to ″10″ for analysis. Morphological identification of EVs was performed by using high-resolution transmission electron microscopy (TEM, JEOL microscope, JSM-7001TA, Tokyo, Japan). Briefly, EVs were added dropwise to the copper mesh and precipitated for 3 min, 5−10 μL of phosphotungstic acid was added dropwise to the copper mesh, precipitated for 3 min, dried at room temperature for 5 min, and imaged under a transmission electron microscope (electron microscope operating voltage 100 kV).

Proteomic Data-dependent Analysis of EVs. We obtained protein lysates by sonication of EV samples and determined protein concentrations (to ensure at least 25 μg of total protein in each sample) using a bicinchoninic acid assay (BCA) kit (Pierce, Rockford IL, USA). Equal amounts of each sample protein were taken for trypsin digestion and were then reduced with 5 mM dithiothreitol for 30 min and alkylated with 11 mM iodoacetamide for 15 min. The alkylated samples were then transferred to ultrafiltration tubes and digested overnight. After trypsin digestion, the peptides were reconstituted in 0.5 M triethylammonium bicarbonate buffer (TEAB). The tryptic peptides were dissolved in 0.1% formic acid and separated using a NanoElute ultrahigh-performance liquid-phase system. The sample was injected into the NSI ion source for ionization and then analyzed with an Exploris480 mass spectrometer. The data acquisition mode used data-dependent scanning (DDA) program. The resulting MS/MS data were processed using the MaxQuant search engine (v.1.5.2.8).

Western Blot. After the RBCs, RBC-EVs, MSCs, and MSC-EVs were lysed with protein RIPA lysis buffer (Beyotime, China), an aBCA protein detection kit (Pierce, Rockford IL, USA) was used to measure the total protein content. The total mass of the cells and EV proteins was 75 μg, and the proteins were separated by SDS−polyacrylamide gel electrophoresis (SDS−PAGE) using a 4% concentration gel and a 10% separation gel. After electrophoresis, the proteins were transferred to PVDF membranes. The membranes were sealed with 5% skim milk powder in Tris-buffered saline containing 0.1% Tween 20 for 1.5 h and then incubated with primary antibodies against SCL4A1, CD63, HSP70, flotillin, CD9, CD81, and calnexin (CANX) (Abcam, England) overnight at 4 °C. The next day, the protein membrane was washed and incubated with a secondary antibody at room temperature for 1.5 h, and the protein bands were detected by a

https://doi.org/10.1021/acsomega.3c06527
ACS Omega 2024, 9, 6492−6504

chemiluminescence kit. Protein imaging was performed using a two-color near-infrared laser imaging system (LI-COR, USA).

SLC4A1-EC Expression Plasmid Construction and Expression. The gene encoding two extracellular regions of SLC4A1 was repeated three times in series and cloned into the pET28b vector (Novagen) at the *Eco*RI and *Ncol* restriction sites. The sequences of SLC4A1-EC are listed in Supporting Information Table 1. The synthetic GSHHHHHH peptide coupled to BSA was used as a negative control for screening. The cDNA sequence of SLC4A1-EC mentioned above was ligated into the pET28b expression vector. After being transformed into the DH5α strain, the positive cloned strain was extracted to obtain sufficient expression plasmid. Double-enzyme digestion verification was performed with *Eco*RI-*Ncol*, and the plasmid was verified by sequencing.

Expression and Purification of SLC4A1-EC Protein. *E. coli* strains T7E and Rosetta (DE3) were transformed with expression plasmids. Bacteria were grown at 37 °C in LB medium containing kanamycin (50 μg/mL). After growing until reaching an OD600 of 0.6, the expression of SLC4A1-EC was induced by adding 0.5 mM IPTG. One group was cultured at 37 °C for 4 h, and the other was cultured at 16 °C for 16 h to optimize the time and temperature of induction expression. Briefly, the bacteria were first expanded and centrifuged at 5000g for 10 min, and the supernatant was discarded. The bacteria were resuspended in lysis buffer (PBS pH 7.5, 10% glycerol), sonicated, and centrifuged at 5000g for 3 min. Aspirate the supernatant into a new EP tube labeled NPE. After centrifugation, the pellet was resuspended in 200 μL of buffer (PBS pH 7.5, 10% glycerol, and 8 M urea) and labeled DPE. Five microliters of loading buffer was added to 20 μL of NPE/DPE samples; then, the samples were heated at 99 °C for 5 min, and SDS−PAGE was performed. After electrophoresis, the separation gel was stained with Coomassie brilliant blue for 2−4 h. Once the gel was dark blue, it was placed into a decolorizing solution for decolorization. The optimal conditions for protein expression were determined according to the results of SDS−PAGE analysis. The sample (DPE) was purified by Ni + NTA resin. The purified target protein was further verified by SDS−PAGE.

Panning of SLC4A1-EC Protein-Specific Anchor Peptides by Phage Display Technology. SLC4A1-EC protein was panned in vitro using 7 and 12 phage display libraries, combinatorial libraries of random 7/12-mer peptides fused to a minor coat protein (pIII) of M13 phage. Each library consists of approximately 109 electroporated (i.e., unique) sequences. In brief, the ELISA plate was coated with 50 μg/mLSLC4A1-EC protein, and then the phage display peptide library was added. After incubation at 37 °C for 1.5 h for complete reaction, the unbound free phages were removed by washing with 0.05% PBST, and the bound phages were eluted with glycine-HCL eluent. The plate was soaked with host *E. coli* and recovered after amplification, followed by another round of screening. After three to four rounds of screening, the recognition of SLC4A1-EC protein was first detected by polyclonal phage ELISA. Then, 96 clones were selected from the plate for monoclonal phage ELISA. The first 10 clones were selected for validation, and the exogenous short peptide sequence carried by the phage clone was identified by high-throughput sequencing.

Conjugation Reactions of Peptides and Proteins. SLC4A1-EC protein (8 μg) was coincubated with peptides XRB2, XRE4, and XRH7 (4 μg) at 37 °C for 1 h, and peptides XRB2, XRE4, and XRH7 alone and SLC4A1-EC protein alone were used as controls. After the reaction, glycerol (final concentration 10%) was added, and the peptide−protein mixture was heated at 99 °C for 15 min for denaturation and then subjected to SDS−PAGE. After electrophoresis, fluorescent protein imaging was first performed on a two-color near-infrared laser imaging system (LI-COR, USA). Then, Coomassie brilliant blue staining was performed for further observation and verification.

Surface Plasmon Resonance. The binding affinity assessment was conducted by using the OpenSPRTM instrument. SLC4A1 served as the ligand, and XRB2, XRE4, and XRH7 were used as analytes. Initially, the buffer was run at a maximum flow rate of 150 μL/min and then adjusted to 20 μL/min once the signal reached baseline. The COOH chip was activated with an EDC/NHS (1:1) solution. First, a 200 μL solution of ligand SLC4A1 diluted with fixed buffer was applied for 4 min, followed by a 200 μL blocking solution. Subsequently, an analyte buffer containing 2% DMSO PBST (pH 7.4) was introduced. A stability check was performed by observing the baseline for 5 min. Then, samples of XRB2, XRE4, and XRH7 analytes were collected at a flow rate of 20 μL/min each, and the protein−peptide binding time lasted for 240 s with a natural dissociation time of 360 s. The surface plasmon resonance (SPR) sensogram data were evaluated with TraceDrawer (Ridgeview Instruments AB, Sweden) evaluation software. The KD values were determined by the one-to-one analysis model.

Binding Affinity of Candidate Peptides on Extracellular Vesicles. To detect the binding ability of peptides XRB2, XRE4, and XRH7 to RBC-EVs, we incubated tetramethylrhodamine (TMR) fluorescent dye-labeled peptides and RBC-EVs for 6 h at 4 °C and then passed the mixture through a 100 kDa centrifugal ultrafilter (Millipore, USA) to remove unbound peptides. The above-grouped samples were incubated with 4 μm aldehyde/sulfuric acid latex beads (Invitrogen, USA) for 15 min at room temperature, blank magnetic beads were set as negative controls, and peptides without ultrafiltration combined with magnetic beads were used as positive controls. The aldehyde/sulfuric acid latex beads contain many aldehyde groups bound to the surface of the polymer particles. The high density of aldehyde groups enables the coupling of RBC-EVs and polypeptides to the latex particles. The fluorescence ratios of different groups were detected by flow cytometry (BD, USA) and observed by fluorescence microscopy. To determine these peptides with MSC-EVs, the CD63 immunopurification of EVs from synovial fluid MSCs was conducted by exosome capture beads (ab239686). The capture beads with the biofluid sample were inverted and placed at 4 °C overnight, and then, the bead-exosomes were recovered in a pellet by low-speed centrifugation. After carefully removing the supernatant, TMR-labeled polypeptides were added for 6 h at 4 °C. A 100 kDa centrifugal ultrafilter (Millipore, USA) was used to remove unbound peptides. The capture antibody beads were suspended in 400 μL of PBS for flow cytometry. Flow cytometry was performed with a combined gate of FSC and SSC to exclude the interference of debris or noise, and 100,000 cells were collected for analysis. To detect PE fluorescence, the excitation wavelength was set to 640 nm, the detector used was FL4, and the filter used was 675/25. The laser scanning confocal microscope (Zeiss LSM 800, Germany) uses a laser channel of 561 nm for capturing images.

https://doi.org/10.1021/acsomega.3c06527
ACS Omega 2024, 9, 6492−6504

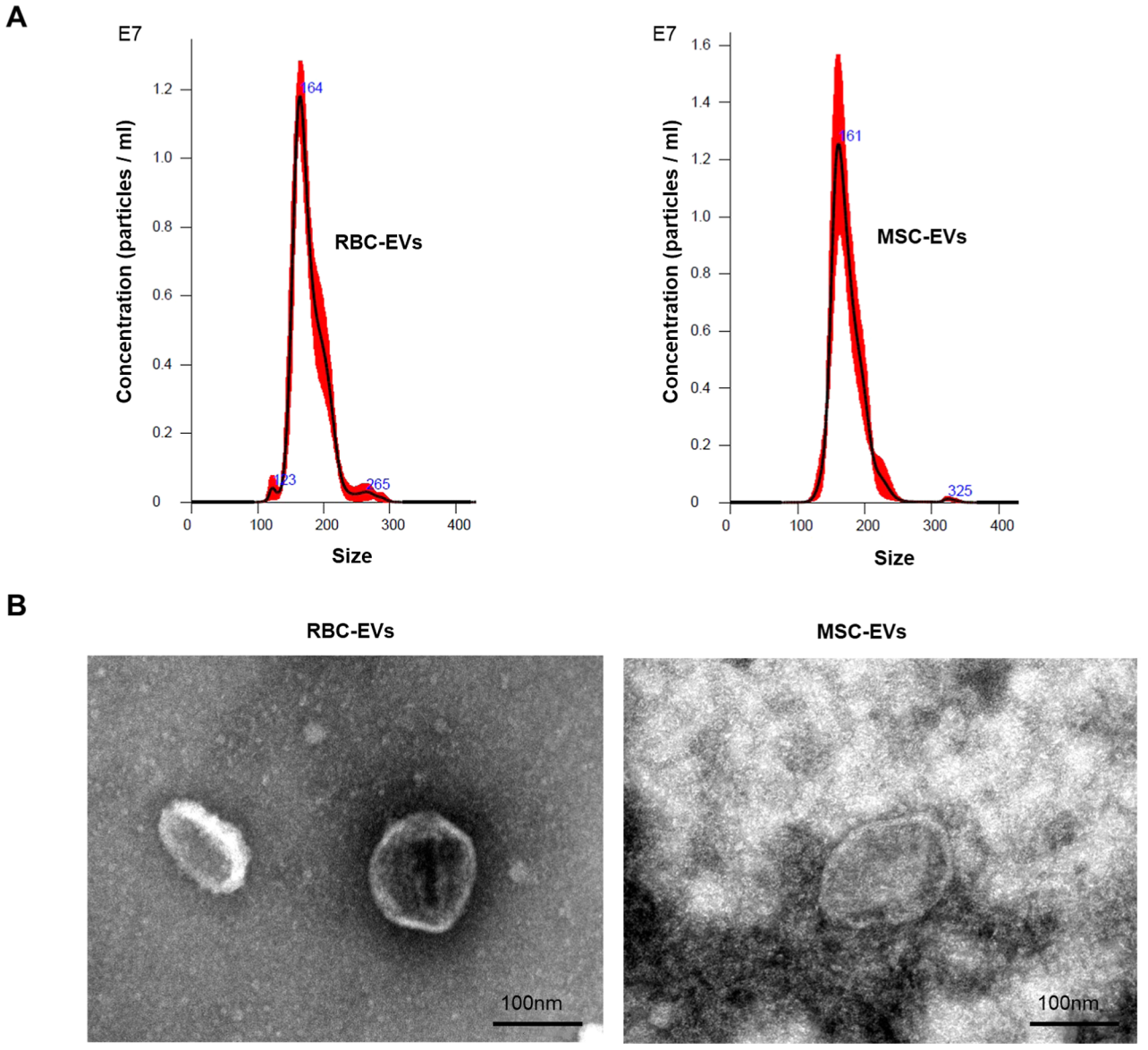

Figure 1. Characterization of EVs. (A) Nanoparticle tracking analysis of the RBC-EVs and MSC-EVs and (B) representative TEM image of the RBC-EVs and MSC-EVs.

In addition, TMR-labeled RBC-EVs or MSC-EVs were collected using exosome spin columns (MW4000). Fluorescence measurements were made by using a Synergy HT Microplate Reader (BioTek Instruments). The binding efficiency of TMR peptides with RBC-EVs or MSC-EVs was calculated by the following formula: Binding efficiency = TMR-peptide-EVs/initial input of TMR-peptide ×100%.

Statistical Analysis. SPSS 23.0 statistical software was used to process experimental data. Statistical significance between two groups was compared using Student's *t*-test, and one-way ANOVA was used to compare multiple groups. $P < 0.05$ was considered statistically significant.

RESULTS

To search for RBC-EV-specific binding peptides, in this study, we compared the proteomics of human RBC-EVs and MSC-EVs and identified the specific highly expressed membrane protein SLC4A1 of RBC-EVs. The specific binding peptides of SLC4A1-EC were screened by phage display technology. The binding sites and binding capacity of SLC4A1 for binding peptides were predicted and evaluated.

High Expression Level of SLC4A1 Protein in RBC-EVs. We collected EVs from human RBCs (n = 3) and human synovial fluid-derived MSCs (n = 3) and characterized the size and morphology of the EVs by nanoparticle tracking analysis (NTA) and TEM (Figure 1A, B). The results showed that the range of the diameter of the RBC-EVs and MSC-EVs was 100−250 nm, and the main peak was approximately 160 nm. The typical cup-shaped morphology was consistent with the morphology of EVs.

We subsequently performed proteomic analysis on the two groups of EVs and identified a total of 1428 proteins, of which 954 contained quantitative information. To identify the purity of EVs, we first examined the expression of EV common marker proteins[23] in the two groups of samples. The results showed that most of the typical EV common proteins were expressed in RBC-EVs and MSC-EVs (Figure 2A). We then performed Pearson correlation coefficient analysis among

https://doi.org/10.1021/acsomega.3c06527
ACS Omega 2024, 9, 6492−6504

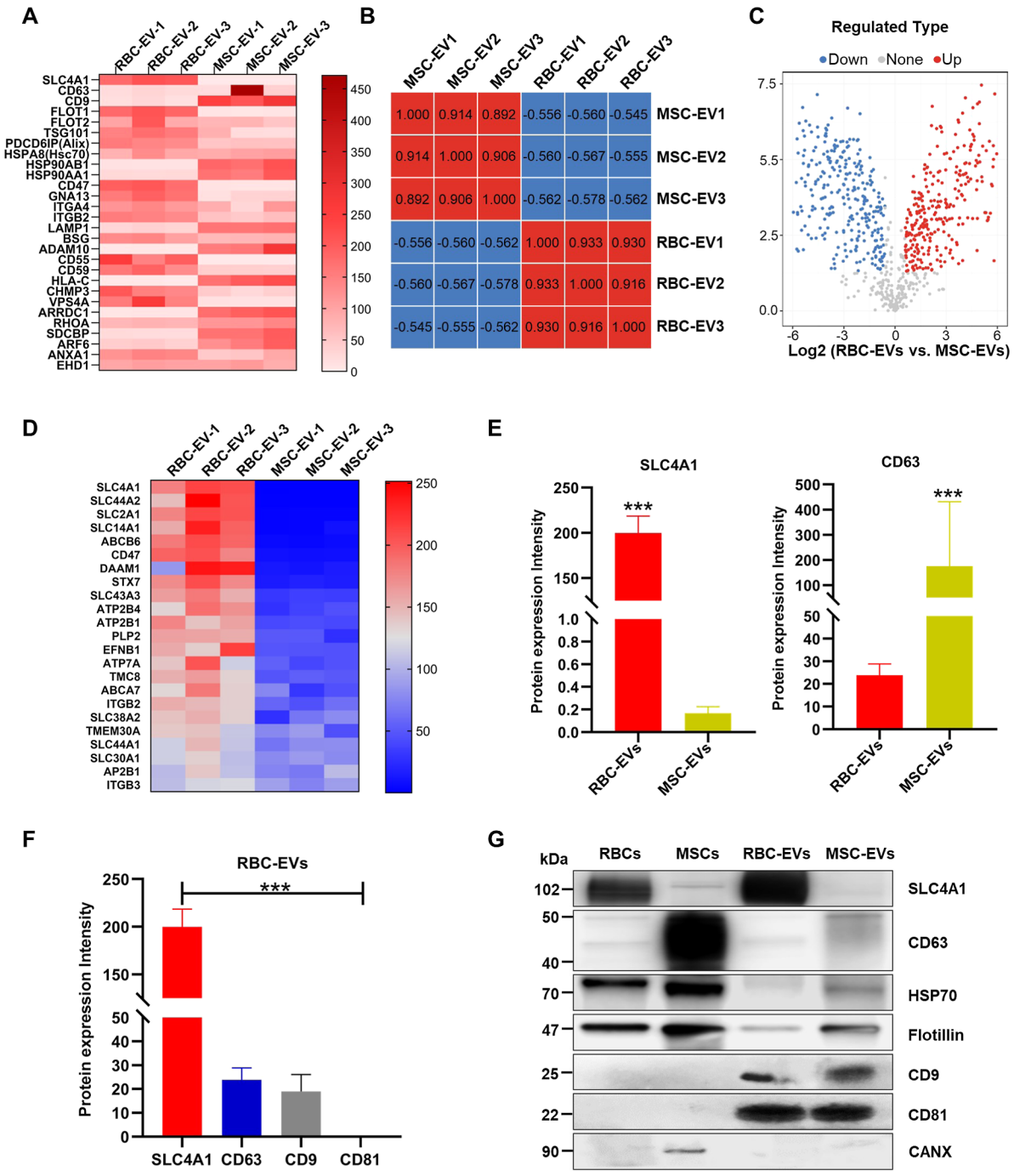

Figure 2. Proteomics comparison and western blot analysis of EVs derived from MSCs and RBCs. (A) Expression of extracellular vesicle markers classically enriched by RBC-EVs and MSC-EVs; (B) Pearson correlation coefficient analysis to evaluate the reproducibility of protein quantification; (C) proteomic volcano plot showing differentially expressed proteins between the RBC-EV and MSC-EV groups; (D) heatmap analysis: compared with MSC-EVs, RBC-EVs had significantly upregulated membrane proteins; (E) quantification of SLC4A1 and CD63 protein expression levels in RBC-EVs and MSC-EVs, *** $p < 0.001$; (F) quantification of SLC4A1, CD63, CD9, and CD81 protein expression levels in RBC-EVs, *** $p < 0.001$; and (G) representative western blot bands of SLC4A1, CD63, and other EV-related proteins in RBC-EVs and MSC-EVs.

samples to evaluate the reproducibility of protein quantification (Figure 2B). The results showed that the Pearson coefficients between the samples in the RBC-EV group or MSC-EV group were both close to 1, while those between the RBC-EV and MSC-EVs group were far from 1, confirming that the reproducibility of protein quantification within the sample groups was better, and there were significant differences in protein expression between the two groups. For the differentially expressed proteins between the two groups, when $P <$ 0.05, the change in the differential expression level was more than 1.5 as the threshold for significant upregulation and less than 1/1.5 as the threshold for significant downregulation. There were many different proteins between the RBC-EV group and the MSC-EV group, among which 302 proteins were upregulated and 340 proteins were downregulated in the RBC-EV group (Figure 2C). To search for membrane proteins that are specifically highly expressed by the RBC-EVs, we further analyzed the membrane proteins that were significantly

https://doi.org/10.1021/acsomega.3c06527
ACS Omega 2024, 9, 6492−6504

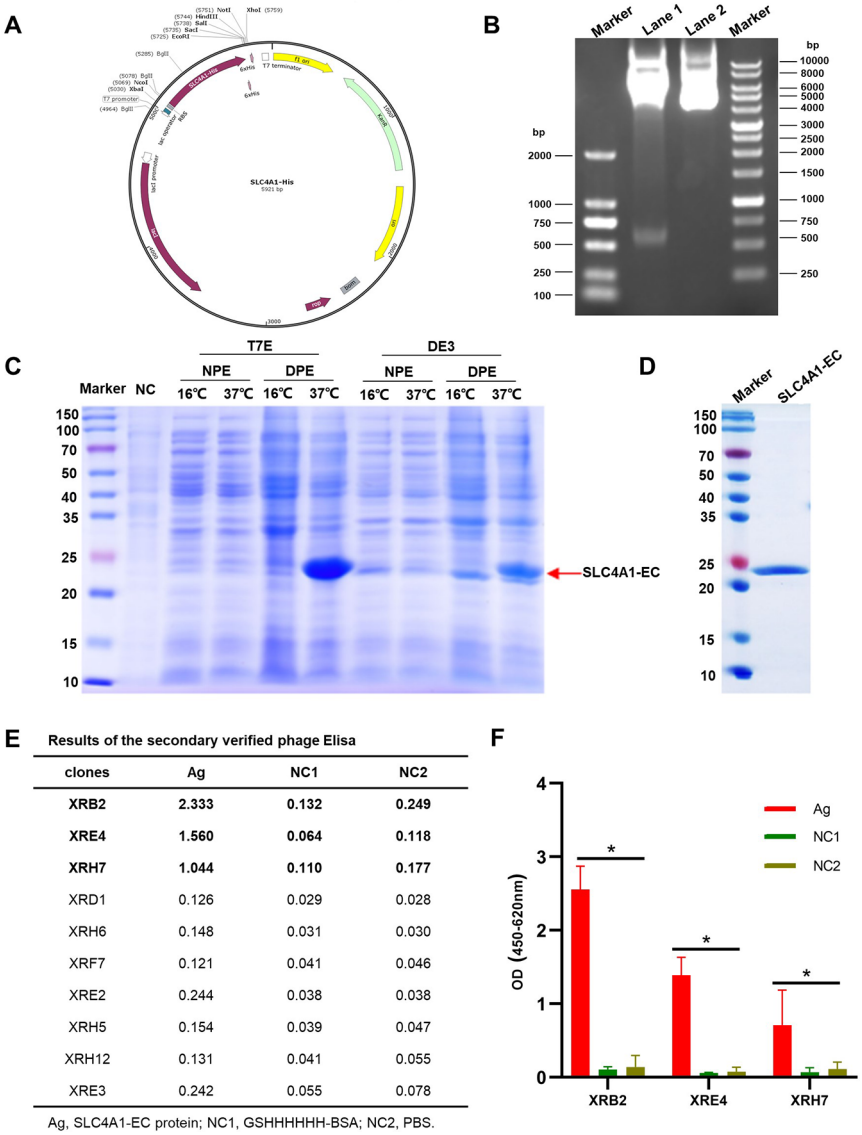

clones	Ag	NC1	NC2
XRB2	**2.333**	**0.132**	**0.249**
XRE4	**1.560**	**0.064**	**0.118**
XRH7	**1.044**	**0.110**	**0.177**
XRD1	0.126	0.029	0.028
XRH6	0.148	0.031	0.030
XRF7	0.121	0.041	0.046
XRE2	0.244	0.038	0.038
XRH5	0.154	0.039	0.047
XRH12	0.131	0.041	0.055
XRE3	0.242	0.055	0.078

Ag, SLC4A1-EC protein; NC1, GSHHHHHH-BSA; NC2, PBS.

Figure 3. Screening of the phage display peptide library against the human SLC4A1-EC protein. (A) Maps of SLC4A1-EC expression plasmids. (B) Verification of the designed plasmid pET28b-SLC4A1-EC. Lane 1: plasmid digested with *Eco*RI and *Nco*I and lane 2: plasmid. (C) Protein gel electrophoresis analysis of SLC4A1-EC expression in the T7E and DE3 strains. NPE: the soluble supernatant after centrifugation of the plasmid-expressing bacteria resuspended in lysis buffer (PBS pH 7.5, 10% glycerol) and DPE: the precipitate after centrifugation was resuspended in 200 μL of buffer (PBS pH 7.5, 10% glycerol, and 8 M urea). (D) SLC4A1-EC protein was obtained by DPE purification. (E) ELISA validation results for the top 10 positive monoclines in phage peptide library screening. (F) Statistical chart of OD (450−620 nm) value of the binding of peptides XRB2, XRE4, and XRH7 to SLC4A1-EC antigen, control peptide, or PBS. Ag: SLC4A1-EC protein, NC1: GSHHHHHH-BSA, NC2: PBS. * $p <$ 0.05.

upregulated in the RBC-EV group compared with the MSC-EV group based on the proteomic data. As shown in Figure 2D, the RBC-EV group had more highly expressed membrane proteins than the MSC-EV group, and the quantification of SLC4A1 protein in the RBC-EV group was significantly higher than that in the MSC-EV group (RBC-EV/MSC-EV = 1256.2, $p < 0.001$), while CD63, the most common membrane protein marker for EVs, was significantly lower in the RBC-EV group than in the MSC-EV group (RBC-EV/MSC-EV = 0.149, $p <$ 0.001) (Figure 2E). In addition, we also compared the protein quantification of SLC4A1 in RBC-EVs and other membrane proteins commonly used in EVs. We found that the quantification of SLC4A1 protein in the RBC-EVs was significantly higher than that of other membrane proteins such as CD63, CD9, and CD81 (Figure 2F). To further verify the increased expression of SLC4A1 in the RBC-EVs, we examined the expression of SLC4A1 protein in the RBC-EVs and MSC-EVs by western blotting and compared the results with those in RBCs and MSCs. Western blot analysis showed that compared with MSCs and MSC-EVs, both RBCs and RBC-EVs showed a higher expression of SLC4A1, and the expression of SLC4A1 in RBC-EVs was higher than that in RBCs, suggesting that SLC4A1 protein was enriched during the release of RBC-EVs. Similar to the quantitative proteomic results, the level of CD63 expression in the RBC-EVs was lower than that in the MSC-EVs. Other EV-related proteins such as HSP70, flotillin, CD9, and CD81 showed little differences in expression between the two groups, while CANX, an endoplasmic reticulum protein, was not expressed in EVs or RBCs (Figure 2G).

https://doi.org/10.1021/acsomega.3c06527
ACS Omega 2024, 9, 6492−6504

A

Name	Displayed peptide Sequences
XRB2	MSMSSIL
XRE4	FASPFYT
XRH7	FQVTGPLTQWGH
XRD1	KIDMLIL
XRH6	FTVGMAW
XRF7	DLTGQRT
XRE2	GVCWMSC
XRH5	WTYDEVD
XRH12	WQPASTP
XRE3	LNDLRHI

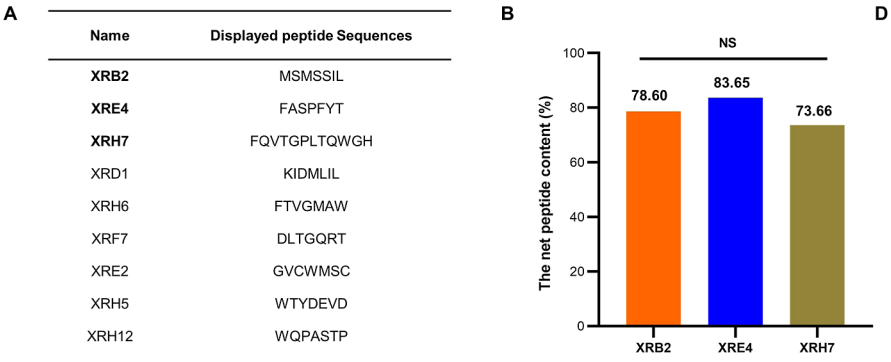

D

Peptides	Protein	KD
XRB2	SLC4A1-EC	141 μM
XRE4	SLC4A1-EC	532 μM
XRH7	SLC4A1-EC	257 μM

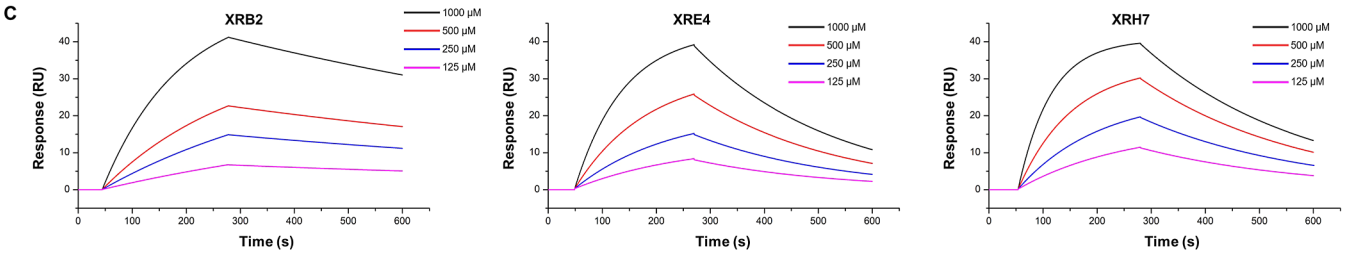

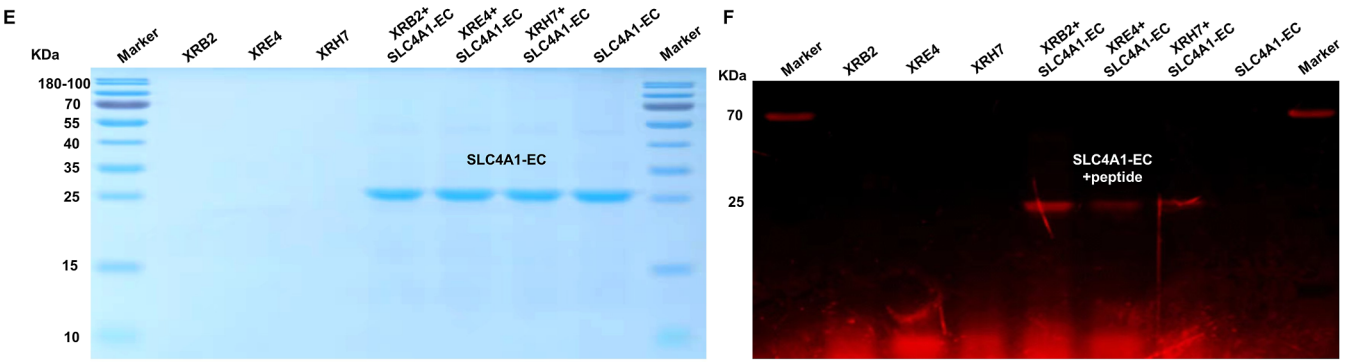

Figure 4. *In vitro* **detection of peptides binding to SLC4A1-EC protein.** (A) 10 candidate peptide sequences screened by phage display technology and (B) statistical chart of net peptide content detection of synthetic peptides XRB2, XRE4, and XRH7. NS, no significance. (C) Affinity between the SLC4A1-EC and XRB2, XRE4, and XRH7 polypeptides (125, 250, 500, and 1000 μM/L) was determined using the SPR method at a flow rate of 20 μL/min. The binding duration between the protein and peptide was 240 s, with a natural dissociation time of 360 s. TraceDrawer analysis software was employed for evaluating the SPR sensing data. (D) KD values were calculated using the one-to-one analysis model. (E) SDS−PAGE gel staining with Coomassie brilliant blue showing SLC4A1-EC protein; (F) fluorescence image showing that the peptide binds to the SLC4A1-EC protein.

Selection and Identification of SLC4A1 Binding Peptides. Human protein SLC4A1 has a total of 911 amino acids (AAs) and 13 transmembrane regions. To use the extracellular segment as the panning source, the amino acids of the two extracellular regions of SLC4A1 were repeated three times in series, 6*His was added to the C-terminus for protein purification, and the protein was labeled SLC4A1-EC. The synthetic GSHHHHHH peptide coupled with BSA was used as a negative control for screening. The SLC4A1-EC protein was then expressed and purified by a mammalian system, but the results indicated that the purity was not high (Supporting Information Figure 1). Therefore, we switched to the *E. coli* system for expression and optimized the culture temperature and time. Protein expression vector pET28b was constructed, as shown in Figure 3A. The obtained expression plasmid was identified by double digestion with *Eco*RI and *Ncol*. The results showed that the size of the target band (SLC4A1-His) was approximately 650 bp, which was in line with expectations (Figure 3B). Then, the optimal expression conditions of SLC4A1-EC protein were found: the T7E strain was incubated at 37 °C for 4 h in precipitation buffer (DPE) (Figure 3C). Finally, the SLC4A1-EC protein with higher purity was obtained after purification (Figure 3D). We then used the purified SLC4A1-EC protein for phage display panning. After multiple rounds of repeated panning and judging that there was specific enrichment, we first performed polyclonal enzyme-linked immunosorbent assay (ELISA) verification and then picked 96 clones for monoclonal ELISA detection. A validated ELISA was performed on positive clones (Figure 3E). The statistical results showed that compared with the control group, the OD values of XRB2, XRE4, and XRH7 combined with SLC4A1-EC were significantly increased (Figure 3F).

In Vitro Verification of the Binding of Panned Peptides to the SLC4A1-EC Protein. To verify whether the panned peptides can bind to the SLC4A1-EC protein, we synthesized three peptides (XRB2, XRE4, and XRH7) based

https://doi.org/10.1021/acsomega.3c06527
ACS Omega 2024, 9, 6492−6504

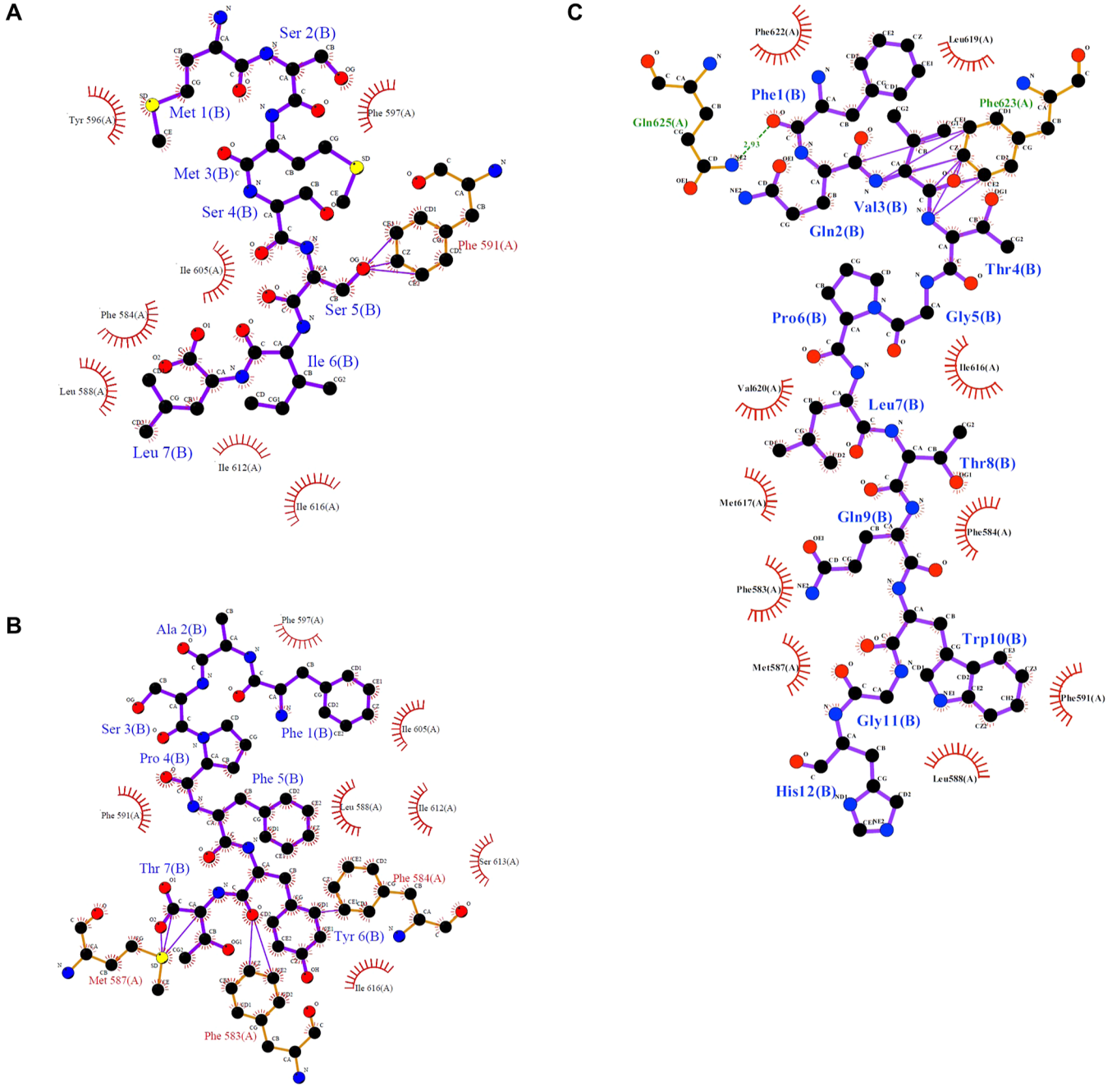

Figure 5. Predicting the binding sites of SLC4A1-EC to the screened anchor peptides XRB2 (A), XRE4 (B), and XRH7 (C). Most of the residues in the peptide−protein binding site are hydrophobic, and three of them (F584, L588, and F591) have a common binding mode with the screened peptides.

on their respective amino acid sequences (Figure 4A, Supporting Information Figure 2). Additionally, the net peptide content of these three peptides was determined. The net peptide content refers to the percentage of peptides in relation to nonpeptide substances, most equilibrium ions, and water. The results revealed that all the three peptides had a net peptide content exceeding 70%, with no significant differences observed among them (Figure 4B), suggesting that subsequent flow and fluorescence detection methods are comparable. Initially, we employed SPR to detect the binding strength between SLC4A1-EC and XRB2, XRE4, and XRH7 peptides. SPR provides real-time sensing information through a sensor, which the instrument converts to response values. Response values increase during binding and decrease during dissociation. The resulting SPR signal generates the sensing map over time (Figure 4C). All obtained data (response value and concentration) were fitted using TraceDrawer software's one-to-one analysis model to get KD values (Figure 4D). The results indicated that SLC4A1-EC exhibited high affinity toward XRB2, XRE4, and XRH7 peptides. Among them, SLC4A1-EC displayed the highest affinity toward XRB2(KD = 141 μM). Furthermore, tetramethylrhodamine (TMR) red fluorophores were added to the N-terminal of each polypeptide before they were incubated with SLC4A1-EC at 37 °C for 1 h. After the protein was denatured, it was detected by SDS−PAGE and stained with Coomassie brilliant blue. The results in

https://doi.org/10.1021/acsomega.3c06527
ACS Omega 2024, 9, 6492−6504

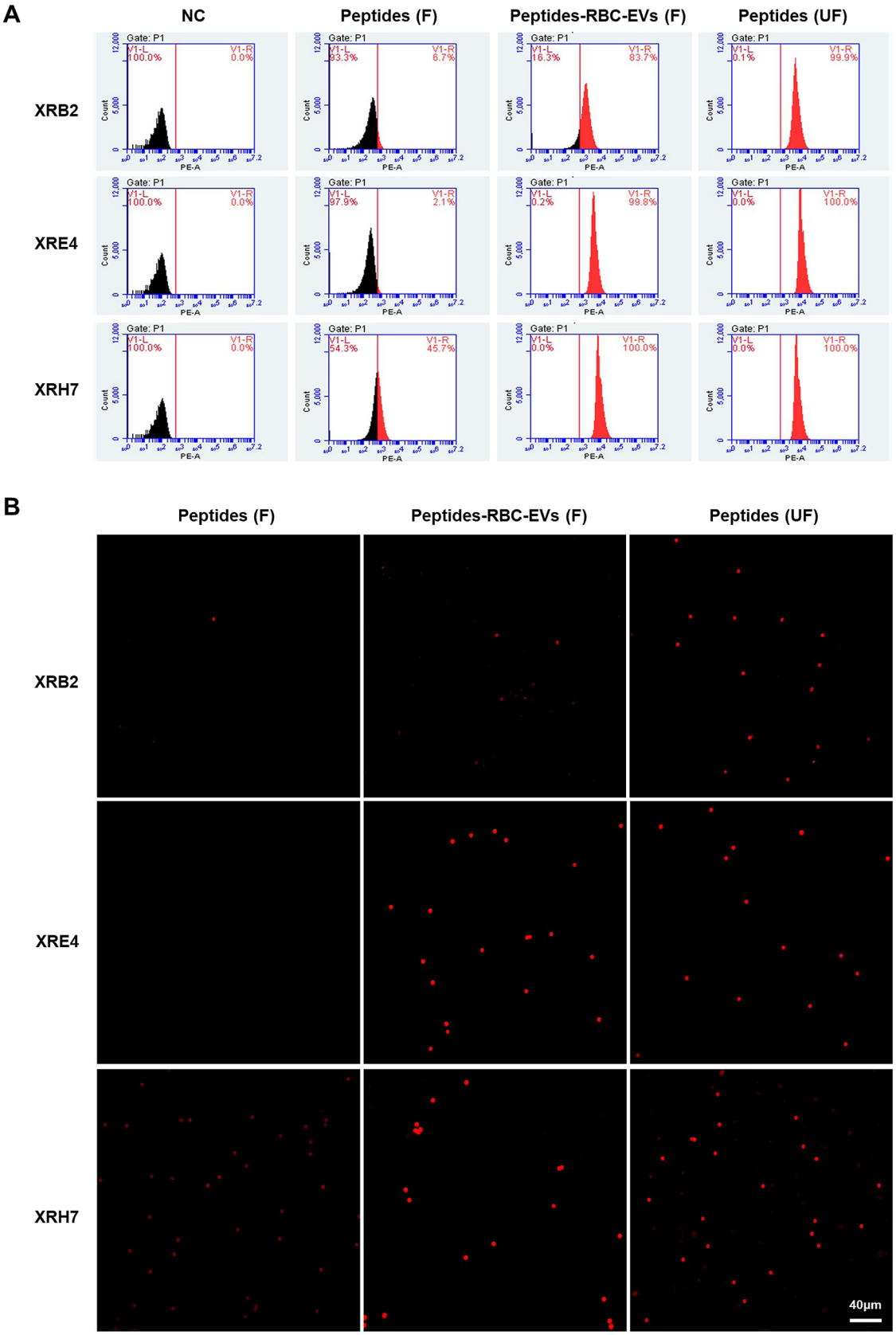

Figure 6. Peptide binding to human RBC-EVs. (A) Flow cytometry was used to detect the binding of XRB2, XRE4, and XRH7 anchor peptides to the RBC-EVs. NC refers to polystyrene beads, which is a negative control. Peptides (F) refer to beads bound to unbound peptides after ultrafiltration. Peptides-RBC-EVs (F) refer to the peptides conjugated by RBC-EVs after ultrafiltration and then conjugated with beads. Peptides (UF) refer to beads bound to peptides without ultrafiltration, as a positive control. (B) Representative fluorescence microscopy images showing TMR-labeled peptides bound to RBC-EVs.

https://doi.org/10.1021/acsomega.3c06527
ACS Omega 2024, 9, 6492−6504

Figure 4E show that the band approximately 25 kDa is the SLC4A1-EC protein. Fluorescent bands could be seen at approximately 25 kDa in the lanes of peptides XRB2, XRE4, and XRH7 incubated with SLC4A1-EC protein. In contrast, we could not detect fluorescent bands in the lanes of the SLC4A1-EC protein or peptides XRB2, XRE4, and XRH7 alone (Figure 4F). These results indicate that peptides XRB2, XRE4, and XRH7 may bind to the SLC4A1-EC protein in vitro.

Molecular Interaction between SLC4A1-EC and Anchor Peptides. This study further analyzed the interactions between SLC4A1-EC and the screened peptides (XRB2, XRE4, and XRH7). Structures of screened peptides were predicted using AlphaFold2[24] and were then docked into SLC4A1 (PDB ID: 4YZF chain A) using ZDOCK.[25] The structural SLC4A1 pictures predicted using AlphaFold2 are shown in the Supporting Information Figure 3. The interface residues of the docked complex were analyzed using LigPlot +[26] and are shown in Figure 5. Peptide XRB2 interacts with SLC4A1-EC through residues F584, L588, F591, Y596, F597, I605, I612, and I616 (Figure 5A). Peptide XRE4 interacts with SLC4A1-EC through residues F583, F584, M587, L588, F591, F597, I605, I612, and S613 (Figure 5B). Peptides XRH7 interact with SLC4A1-EC through residues F583, F584, M587, L588, F591, I616, M617, L619, V620, F622, F623, and N625 (Figure 5C). Most of those residues are hydrophobic, and three residues (F584, L588, and F591) are shared by XRB2, XRE4, and XRH7, indicating that those residues are hotspot regions for peptide screening in the ectodomain of SLC4A1.

In Vitro Detection of the Binding of Panned Peptides to the Human RBC-EV Surface. To further test whether peptides XRB2, XRE4, and XRH7 can bind to the SLC4A1 protein on the surface of RBC-EVs, we incubated equal amounts of TMR-labeled XRB2, XRE4, and XRH7 peptides with the RBC-EVs for 6 h at 4 °C and then transferred the mixture to an ultrafiltration tube to remove unbound peptides after continuous ultrafiltration. The conjugates of peptides and RBC-EVs (peptides-RBC-EVs (F)) and filtered unbound peptides (peptides (F)) were incubated with polystyrene beads, and blank polystyrene beads were used as negative controls (NC). The coincubation solution of simple peptides and polystyrene beads was used as a positive control (peptides (UF)). Flow cytometry and fluorescence microscopy were used to detect the binding of the peptides to the RBC-EVs. Flow cytometry results showed that TMR-labeled XRB2, XRE4, and XRH7 peptides could bind to RBC-EVs, but the positive rate of XRE4 and XRH7 binding was higher than that of XRB2. Nevertheless, the positive ratio of unbound XRH7 was also significantly higher than those of XRB2 and XRE4 (Figure 6A, Supporting Information Figure 4A, B). Consistent with the flow cytometry results, the fluorescence results suggested that peptides XRB2, XRE4, and XRH7 could bind to RBC-EVs, but they have different binding capacities (Figure 6B).

To further demonstrate that XRB2, XRE4, and XRH7 could specifically bind to RBC-EVs, we captured MSC-EVs using exosome capture beads and then coincubated them with TMR-labeled peptides, and flow analysis of peptides with MSC-EV conjugates showed that this interaction was less successful in MSC-EVs (Supporting Information Figure 4C). In addition, we calculated the binding of XRB2, XRE4, and XRH7 to RBC-EVs or MSC-EVs using fluorescence. The results suggested that the binding rate of RBC-EVs to peptides was significantly higher than that of MSC-EVs. Moreover, XRE4 showed stronger binding to RBC-EVs than XRB2 and XRH7 (Supporting Information Figure 4D).

Discussion. In this study, we analyzed the proteomes of RBC-derived and MSC-derived EVs and screened a membrane protein, SLC4A1, with a highly specific expression in RBC-EVs. To identify an SLC4A1-specific peptide, we purified the extracellular segment of the SLC4A1 protein and identified the SLC4A1-specific binding peptide using phage display technology. Additionally, we identified the binding ability of three peptides, XRB2, XRE4, and XRH7, to both the SLC4A1-EC protein and RBC-EVs. These RBC-EV-anchor peptides can be modified by other homing peptides, which can target specific cells, tissues, or organs.

Currently, RBC-EVs have attracted increasing attention in the field of drug delivery due to their unique advantages. A study showed that nearly half of the leukemia cells remained in mice treated with RBC-EV-delivered ASOs (antisense oligonucleotides) by tail vein injection, and many EVs accumulated in other organs.[27] This result suggests the importance of targeting specific cells with RBC-EVs. EVs are selectively enriched in some transmembrane proteins that can display ligands/homing peptides on their surface, which could confer RBC-EV targeting capability.[28] Our study showed that compared with MSC-EVs, common exosomal membrane proteins, such as CD63 and CD9, were expressed less in RBC-EVs, while SLC4A1 was expressed more specifically. Then, we screened the peptides that specifically bind to the extracellular segment of the membrane protein SLC4A1 using phage display technology. Phage display technology has been widely used in the screening of cell-targeted peptides since the Smith report in 1985.[29,30] Compared with other modification methods that directly confer EVs with targeting, such as common bioconjugation and click chemistry reactions, which may impair EV function by altering or obscuring the active site of modified surface proteins. Additionally, multivalent electrostatic interactions may increase EV toxicity through membrane thinning and hole formation.[31] Therefore, there is an increased need to identify more specific EV anchor peptides via phage display technology. We found that XRB2, XRE4, and XRH7 had strong binding ability to SLC4A1-EC by phage display technology. Among them, XRB2 has the most vital binding ability, and further in vitro experimental verification results also suggested that XRB2 has a stronger binding ability to SLC4A1-EC. In addition, when the binding of XRB2, XRE4, and XRH7 to RBC-EVs and MSC-EVs was tested, these peptides were found to have strong binding ability to RBC-EVs, with XRE4 binding capacity to RBC-EVs being more specific. This may be related to the spatial conformation of SLC4A1 on the RBC-EV surface.

The connection of EVs to their surface protein-anchored peptides has broad application prospects. Nguyen A.et al. used purified EVs as bait for screening a phage display peptide library. Once identified, the selected peptides could be used for EV isolation.[32] Iaccino E. et al. selected Id peptides by screening a phage display library to bait the Ig-BCR expressed by 5T33MM cells. By FACS, FITC-conjugated Id peptides detected MM-released exosomes in the serum of 5T33MM-engrafted mice earlier than serum paraprotein, and the level of MM-released exosomes was correlated with tumor progression.[33] In addition, by phage display technology, Gao X. et al. identified exosome membrane protein CD63 as a specific anchor peptide, CP05. CP05 modifications did not alter the

https://doi.org/10.1021/acsomega.3c06527
ACS Omega 2024, 9, 6492−6504

exosome morphology, size, or tissue distribution. Approximately 77% of the peptide remained intact after 6 h in serum. This indicates that modifying EVs with anchor peptides screened by phage display technology is a safe and stable method. CP05 can not only capture exosomes from serum for disease diagnosis but can also be simultaneously coupled with muscle targeting peptide M12 and drug phosphorodiamidate morpholino oligomer (PMO) for treatment of Duchenne muscular dystrophy (DMD).[17] However, our study still has some limitations. We will further investigate the tissue distribution, metabolic time, serum immune indices, and organ structure changes in mice treated with anchored peptide-modified RBC-EVs to clarify the safety and stability of the anchored peptide. In addition, the binding of the screened polypeptides to RBC-EVs has only been preliminarily verified, and further experimental studies are still needed to determine their functions, such as isolating RBC-EVs in serum and targeting the delivery of drugs.

CONCLUSIONS

We identified the highly expressed membrane protein SLC4A1 specific for RBC-EV and screened the specific binding peptides XRB2, XRE4, and XRH7 for SLC4A1 using phage display technology. RBC-EV's binding sites and efficiency with different binding peptides were preliminarily predicted and evaluated. The discovery of RBC-EV-specific anchoring peptides provides a novel strategy for targeted drug delivery therapy. However, it is essential to note that further verification of the interaction between polypeptides and RBC-EVs through peripheral blood or in vivo experiments and stability detection is necessary.

ASSOCIATED CONTENT

Data Availability Statement

The data supporting this study can be accessed in the published article and its online Supporting Information.

Supporting Information

The Supporting Information is available free of charge at https://pubs.acs.org/doi/10.1021/acsomega.3c06527.

Gene coding and amino acid sequence of SLC4A1-EC; expression and purification of SLC4A1-EC protein by a mammalian expression system; mass spectrum identification of peptide synthesis; structural full pictures of SLC4A1 predicted by AlphaFold2; and binding detection of XRB2, XRE4, and XRH7 anchor peptides to RBC-EVs or MSC-EVs (PDF)

AUTHOR INFORMATION

Corresponding Authors

Yujie Liang − *Department of Child and Adolescent Psychiatry, Shenzhen Institute of Mental Health, Shenzhen Mental Health Center, ShenzhenKangning Hospital, Shenzhen 518020 Guangdong, China;* orcid.org/0000-0002-0860-4859; Email: liangyjie@126.com

Li Duan − *Department of Orthopedics, the First Affiliated Hospital of Shenzhen University, Shenzhen Second People's Hospital, Guangdong Provincial Research Center for Artificial Intelligence and Digital Orthopedic Technology, Shenzhen 518035 Guangdong, China*; Email: duanl@szu.edu.cn

Authors

Limei Xu − *Department of Orthopedics, the First Affiliated Hospital of Shenzhen University, Shenzhen Second People's Hospital, Guangdong Provincial Research Center for Artificial Intelligence and Digital Orthopedic Technology, Shenzhen 518035 Guangdong, China; Affiliated Hospital of Jining Medical University, Jining Medical University, Jining 272029 Shandong, China;* orcid.org/0000-0003-0391-7327

Xiao Xu − *Department of Orthopedics, the First Affiliated Hospital of Shenzhen University, Shenzhen Second People's Hospital, Guangdong Provincial Research Center for Artificial Intelligence and Digital Orthopedic Technology, Shenzhen 518035 Guangdong, China; Affiliated Hospital of Jining Medical University, Jining Medical University, Jining 272029 Shandong, China*

Jiang Xia − *Department of Chemistry, The Chinese University of Hong Kong, Shatin 999077 Hong Kong SAR, China;* orcid.org/0000-0001-8112-7625

Huawei Zhang − *Shenzhen Institute of Advanced Technology, Chinese Academy of Sciences, Shenzhen 518055 Guangdong, China; Department of Biomedical Engineering, South University of Science and Technology of China, Shenzhen 518055 Guangdong, China*

Complete contact information is available at: https://pubs.acs.org/10.1021/acsomega.3c06527

Author Contributions

Limei Xu, Yujie Liang, and Li Duan were involved in the conception and design; Limei Xu, Xiao Xu, and Huawei Zhang analyzed and interpreted the data; Limei Xu drafted the paper, Jiang Xia revised it critically for intellectual content; Yujie Liang and Li Duan approved the final version to be published; and all authors agree to be accountable for all aspects of the work.

Funding

This project was supported by the National Natural Science Foundation of China (81972116, 81772394, 82372269, and 31900046); the Shenzhen Science and Technology Projects (SGDX20201103095800003, GJHZ20200731095606019, and JCYJ20170817172023838); the Guangdong International Cooperation Project (2021A0505030011); the Shenzhen Fund for Guangdong Provincial High Level Clinical Key Specialties (no. SZGSP013), the Shenzhen Key Medical Discipline Construction Fund (no. SZXK042), the Medical-Engineering Interdisciplinary Research Foundation of Shenzhen University (no. 2023YG014), the Shandong Provincial Natural Science Foundation (ZR2023QH148), and the PhD Research Foundation of Affiliated Hospital of Jining Medical University (2022-BS-04).

Notes

The authors declare no competing financial interest.

ACKNOWLEDGMENTS

The authors convey their thanks to everyone who contributed to this article.

REFERENCES

(1) van Niel, G.; D'Angelo, G.; Raposo, G. Shedding light on the cell biology of extracellular vesicles. *Nat. Rev. Mol. Cell Biol.* **2018**, *19* (4), 213−228.

(2) Liang, Y.; Iqbal, Z.; Wang, J.; Xu, L.; Xu, X.; Ouyang, K.; Zhang, H.; Lu, J.; Duan, L.; Xia, J. Cell-derived extracellular vesicles for

CRISPR/Cas9 delivery: engineering strategies for cargo packaging and loading. *Biomater. Sci.* **2022**, *10* (15), 4095−4106.
(3) Duan, L.; Xu, L.; Xu, X.; Qin, Z.; Zhou, X.; Xiao, Y.; Liang, Y.; Xia, J. Exosome-mediated delivery of gene vectors for gene therapy. *Nanoscale* **2021**, *13* (3), 1387−1397.
(4) Xu, X.; Xu, L.; Wen, C.; Xia, J.; Zhang, Y.; Liang, Y. Programming assembly of biomimetic exosomes: An emerging theranostic nanomedicine platform. *Mater. Today Bio* **2023**, *22*, 100760.
(5) Liang, Y.; Iqbal, Z.; Lu, J.; Wang, J.; Zhang, H.; Chen, X.; Duan, L.; Xia, J. Cell-derived nanovesicle-mediated drug delivery to the brain: Principles and strategies for vesicle engineering. *Mol. Ther.* **2023**, *31* (5), 1207−1224.
(6) Xu, X.; Liang, Y.; Li, X.; Ouyang, K.; Wang, M.; Cao, T.; Li, W.; Liu, J.; Xiong, J.; Li, B.; Xia, J.; Wang, D.; Duan, L. Exosome-mediated delivery of kartogenin for chondrogenesis of synovial fluid-derived mesenchymal stem cells and cartilage regeneration. *Biomaterials* **2021**, *269*, 120539.
(7) Tang, Y.; Zhou, Y.; Li, H. J. Advances in mesenchymal stem cell exosomes: a review. *Stem Cell Res. Ther.* **2021**, *12* (1), 71.
(8) Xu, X.; Xu, L.; Xia, J.; Wen, C.; Liang, Y.; Zhang, Y. Harnessing knee joint resident mesenchymal stem cells in cartilage tissue engineering. *Acta Biomater.* **2023**, *168*, 372−387.
(9) Sun, Y.; Liu, G.; Zhang, K.; Cao, Q.; Liu, T.; Li, J. Mesenchymal stem cells-derived exosomes for drug delivery. *Stem Cell Res. Ther.* **2021**, *12* (1), 561.
(10) Shi, J.; Kundrat, L.; Pishesha, N.; Bilate, A.; Theile, C.; Maruyama, T.; Dougan, S. K.; Ploegh, H. L.; Lodish, H. F. Engineered red blood cells as carriers for systemic delivery of a wide array of functional probes. *Proc. Natl. Acad. Sci. USA* **2014**, *111* (28), 10131−10136.
(11) Peng, B.; Nguyen, T. M.; Jayasinghe, M. K.; Gao, C.; Pham, T. T.; Vu, L. T.; Yeo, E.; Yap, G.; Wang, L.; Goh, B. C.; Tam, W. L.; Luo, D.; Le, M. T. Robust delivery of RIG-I agonists using extracellular vesicles for anti-cancer immunotherapy. *J. Extracell. Vesicles* **2022**, *11* (4), No. e12187.
(12) Liang, Y.; Duan, L.; Lu, J.; Xia, J. Engineering exosomes for targeted drug delivery. *Theranostics* **2021**, *11* (7), 3183−3195.
(13) Liang, Y.; Xu, X.; Xu, L.; Iqbal, Z.; Ouyang, K.; Zhang, H.; Wen, C.; Duan, L.; Xia, J. Chondrocyte-specific genomic editing enabled by hybrid exosomes for osteoarthritis treatment. *Theranostics* **2022**, *12* (11), 4866−4878.
(14) Duan, L.; Ouyang, K.; Wang, J.; Xu, L.; Xu, X.; Wen, C.; Xie, Y.; Liang, Y.; Xia, J. Exosomes as Targeted Delivery Platform of CRISPR/Cas9 for Therapeutic Genome Editing. *Chembiochem* **2021**, *22* (24), 3360−3368.
(15) Xu, X.; Iqbal, Z.; Xu, L.; Wen, C.; Duan, L.; Xia, J.; Yang, N.; Zhang, Y.; Liang, Y. Brain-derived extracellular vesicles: Potential diagnostic biomarkers for central nervous system diseases. *Psychiatry Clin. Neurosci.* **2023**, *38*, 1585−1597.
(16) Xu, L.; Liang, Y.; Xu, X.; Xia, J.; Wen, C.; Zhang, P.; Duan, L. Blood cell-derived extracellular vesicles: diagnostic biomarkers and smart delivery systems. *Bioengineered* **2021**, *12* (1), 7929−7940.
(17) Gao, X.; Ran, N.; Dong, X.; Zuo, B.; Yang, R.; Zhou, Q.; Moulton, H. M.; Seow, Y.; Yin, H. Anchor peptide captures, targets, and loads exosomes of diverse origins for diagnostics and therapy. *Sci. Transl. Med.* **2018**, *10* (444), No. eaat0195.
(18) Xu, L.; Xu, X.; Liang, Y.; Wen, C.; Ouyang, K.; Huang, J.; Xiao, Y.; Deng, X.; Xia, J.; Duan, L. Osteoclast-targeted delivery of anti-miRNA oligonucleotides by red blood cell extracellular vesicles. *J. Controlled Release* **2023**, *358*, 259−272.
(19) Andreu, Z.; Yanez-Mo, M. Tetraspanins in extracellular vesicle formation and function. *Front. Immunol.* **2014**, *5*, 442.
(20) Hoshino, A.; Kim, H. S.; Bojmar, L.; Gyan, K. E.; Cioffi, M.; Hernandez, J.; Zambirinis, C. P.; Rodrigues, G.; Molina, H.; Heissel, S.; Mark, M. T.; Steiner, L.; Benito-Martin, A.; Lucotti, S.; Di Giannatale, A.; Offer, K.; Nakajima, M.; Williams, C.; Nogues, L.; Pelissier Vatter, F. A.; Hashimoto, A.; Davies, A. E.; Freitas, D.; Kenific, C. M.; Ararso, Y.; Buehring, W.; Lauritzen, P.; Ogitani, Y.; Sugiura, K.; Takahashi, N.; Aleckovic, M.; Bailey, K. A.; Jolissant, J. S.; Wang, H.; Harris, A.; Schaeffer, L. M.; Garcia-Santos, G.; Posner, Z.; Balachandran, V. P.; Khakoo, Y.; Raju, G. P.; Scherz, A.; Sagi, I.; Scherz-Shouval, R.; Yarden, Y.; Oren, M.; Malladi, M.; Petriccione, M.; De Braganca, K. C.; Donzelli, M.; Fischer, C.; Vitolano, S.; Wright, G. P.; Ganshaw, L.; Marrano, M.; Ahmed, A.; DeStefano, J.; Danzer, E.; Roehrl, M.; Lacayo, N. J.; Vincent, T. C.; Weiser, M. R.; Brady, M. S.; Meyers, P. A.; Wexler, L. H.; Ambati, S. R.; Chou, A. J.; Slotkin, E. K.; Modak, S.; Roberts, S. S.; Basu, E. M.; Diolaiti, D.; Krantz, B. A.; Cardoso, F.; Simpson, A. L.; Berger, M.; Rudin, C. M.; Simeone, D. M.; Jain, M.; Ghajar, C. M.; Batra, S. K.; Stanger, B. Z.; Bui, J.; Brown, K. A.; Rajasekhar, V. K.; Healey, J. H.; de Sousa, M.; Kramer, K.; Sheth, S.; Baisch, J.; Pascual, V.; Heaton, T. E.; La Quaglia, M. P.; Pisapia, D. J.; Schwartz, R.; Zhang, H.; Liu, Y.; Shukla, A.; Blavier, L.; DeClerck, Y. A.; LaBarge, M.; Bissell, M. J.; Caffrey, T. C.; Grandgenett, P. M.; Hollingsworth, M. A.; Bromberg, J.; Costa-Silva, B.; Peinado, H.; Kang, Y.; Garcia, B. A.; O'Reilly, E. M.; Kelsen, D.; Trippett, T. M.; Jones, D. R.; Matei, I. R.; Jarnagin, W. R.; Lyden, D. Extracellular Vesicle and Particle Biomarkers Define Multiple Human Cancers. *Cell* **2020**, *182* (4), 1044.
(21) Arakawa, T.; Kobayashi-Yurugi, T.; Alguel, Y.; Iwanari, H.; Hatae, H.; Iwata, M.; Abe, Y.; Hino, T.; Ikeda-Suno, C.; Kuma, H.; Kang, D.; Murata, T.; Hamakubo, T.; Cameron, A. D.; Kobayashi, T.; Hamasaki, N.; Iwata, S. Crystal structure of the anion exchanger domain of human erythrocyte band 3. *Science* **2015**, *350* (6261), 680−684.
(22) Jia, Z.; Liang, Y.; Xu, X.; Li, X.; Liu, Q.; Ou, Y.; Duan, L.; Zhu, W.; Lu, W.; Xiong, J.; Wang, D. Isolation and characterization of human mesenchymal stem cells derived from synovial fluid by magnetic-activated cell sorting (MACS). *Cell Biol. Int.* **2018**, *42* (3), 262−271.
(23) Poupardin, R.; Wolf, M.; Strunk, D. Adherence to minimal experimental requirements for defining extracellular vesicles and their functions. *Adv. Drug Delivery Rev.* **2021**, *176*, 113872.
(24) Jumper, J.; Evans, R.; Pritzel, A.; Green, T.; Figurnov, M.; Ronneberger, O.; Tunyasuvunakool, K.; Bates, R.; Zidek, A.; Potapenko, A.; Bridgland, A.; Meyer, C.; Kohl, S.; Ballard, A. J.; Cowie, A.; Romera-Paredes, B.; Nikolov, S.; Jain, R.; Adler, J.; Back, T.; Petersen, S.; Reiman, D.; Clancy, E.; Zielinski, M.; Steinegger, M.; Pacholska, M.; Berghammer, T.; Bodenstein, S.; Silver, D.; Vinyals, O.; Senior, A. W.; Kavukcuoglu, K.; Kohli, P.; Hassabis, D. Highly accurate protein structure prediction with AlphaFold. *Nature* **2021**, *596* (7873), 583−589.
(25) Pierce, B. G.; Wiehe, K.; Hwang, H.; Kim, B. H.; Vreven, T.; Weng, Z. ZDOCK server: interactive docking prediction of protein-protein complexes and symmetric multimers. *Bioinformatics* **2014**, *30* (12), 1771−1773.
(26) Laskowski, R. A.; Swindells, M. B. LigPlot+: multiple ligand-protein interaction diagrams for drug discovery. *J. Chem. Inf. Model.* **2011**, *51* (10), 2778−2786.
(27) Usman, W. M.; Pham, T. C.; Kwok, Y. Y.; Vu, L. T.; Ma, V.; Peng, B.; Chan, Y. S.; Wei, L.; Chin, S. M.; Azad, A.; He, A. B.; Leung, A.; Yang, M.; Shyh-Chang, N.; Cho, W. C.; Shi, J.; Le, M. T. N. Efficient RNA drug delivery using red blood cell extracellular vesicles. *Nat. Commun.* **2018**, *9* (1), 2359.
(28) Xitong, D.; Xiaorong, Z. Targeted therapeutic delivery using engineered exosomes and its applications in cardiovascular diseases. *Gene* **2016**, *575* (2), 377−384.
(29) Smith, G. P. Filamentous fusion phage: novel expression vectors that display cloned antigens on the virion surface. *Science* **1985**, *228* (4705), 1315−1317.
(30) Saw, P. E.; Song, E. W. Phage display screening of therapeutic peptide for cancer targeting and therapy. *Protein Cell* **2019**, *10* (11), 787−807.
(31) Armstrong, J. P.; Holme, M. N.; Stevens, M. M. Re-Engineering Extracellular Vesicles as Smart Nanoscale Therapeutics. *ACS Nano* **2017**, *11* (1), 69−83.

https://doi.org/10.1021/acsomega.3c06527
ACS Omega 2024, 9, 6492−6504

(32) Nguyen, A.; Wang, T.; Turko, I. V. Quantitative proteomic analysis for evaluating affinity isolation of extracellular vesicles. *J. Proteonomics* **2021**, *249*, 104359.
(33) Iaccino, E.; Mimmi, S.; Dattilo, V.; Marino, F.; Candeloro, P.; Di Loria, A.; Marimpietri, D.; Pisano, A.; Albano, F.; Vecchio, E.; Ceglia, S.; Golino, G.; Lupia, A.; Fiume, G.; Quinto, I.; Scala, G. Monitoring multiple myeloma by idiotype-specific peptide binders of tumor-derived exosomes. *Mol. Cancer* **2017**, *16* (1), 159.

https://doi.org/10.1021/acsomega.3c06527
ACS Omega 2024, 9, 6492−6504